

Latent Wavelet Diffusion: Enabling 4K Image Synthesis for Free

Luigi Sigillo^{1,2*} Shengfeng He² Danilo Comminiello¹

¹Sapienza University of Rome

²Singapore Management University

luigi.sigillo@uniroma1.it

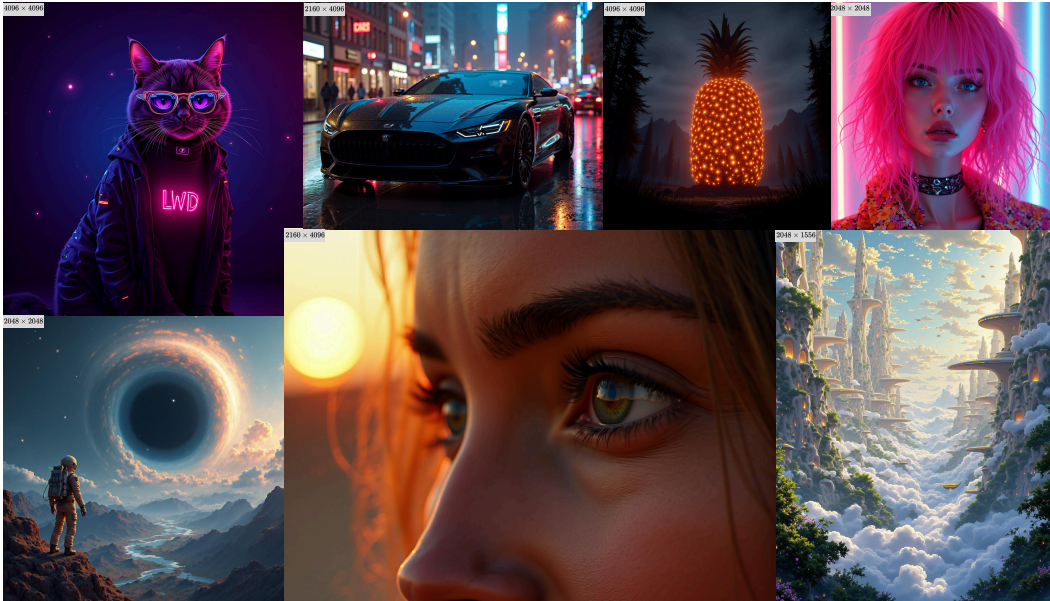


Figure 1: We propose Latent Wavelet Diffusion, achieving 4K image synthesis without architectural changes or additional inference cost to existing latent diffusion models.

Abstract

High-resolution image synthesis remains a core challenge in generative modeling, particularly in balancing computational efficiency with the preservation of fine-grained visual detail. We present *Latent Wavelet Diffusion (LWD)*, a lightweight framework that enables any latent diffusion model to scale to ultra-high-resolution image generation (2K to 4K) for free. LWD introduces three key components: (1) a scale-consistent variational autoencoder objective that enhances the spectral fidelity of latent representations; (2) wavelet energy maps that identify and localize detail-rich spatial regions within the latent space; and (3) a time-dependent masking strategy that focuses denoising supervision on high-frequency components during training. LWD requires no architectural modifications and incurs no additional computational overhead. Despite its simplicity, it consistently improves perceptual quality and reduces FID in ultra-high-resolution image synthesis, outperforming strong baseline models. These results highlight the effectiveness of frequency-aware, signal-driven supervision as a principled and efficient approach for high-resolution generative modeling.

*Corresponding author.

1 Introduction

Diffusion models have become a dominant paradigm in generative modeling, achieving state-of-the-art results in tasks such as image synthesis [43, 49, 37, 63], super-resolution [48, 54, 61], and image editing [7, 39]. Foundational methods like Denoising Diffusion Probabilistic Models (DDPM) [22] and Denoising Diffusion Implicit Models (DDIM) [56] have enabled increasingly powerful variants. Latent Diffusion Models (LDMs) [47] improve efficiency by operating in a learned latent space, while recent architectures such as Diffusion Transformers (DiTs) [41, 13] further enhance scalability and modeling capacity.

Despite recent advances, generating ultra-high-resolution (UHR) images at resolutions of 2K to 4K and beyond remains a significant challenge. Simply scaling models trained on lower-resolution data often fails to generalize, leading to repeated structures, blurred textures, and spatial inconsistencies [4, 20]. Naive alternatives, such as hierarchical generation pipelines and post-hoc super-resolution techniques [11, 20], typically produce oversmoothed outputs. To overcome these limitations, several strategies have been explored. One direction involves direct UHR training or fine-tuning [46, 9], although this typically demands extensive computational resources, access to proprietary high-resolution datasets [36], and substantial GPU memory for large model backbones [31, 13]. Other efforts focus on architectural modifications to improve long-range dependency modeling [35], or optimization techniques that enhance the quality of latent representations [19].

Across these varied approaches, a common limitation persists: most methods treat all spatial regions uniformly during generation, applying the same refinement process to areas with vastly different visual complexity. This uniformity disregards local frequency variation, failing to distinguish between smooth regions and areas rich in textures, edges, or semantic structure. The consequences are twofold. First, computation is wasted on low-detail areas that require minimal refinement. Second, high-detail regions are not sufficiently supervised, leading to artifacts or loss of fidelity. These issues stem from both architectural and algorithmic constraints: latent representations often lack the structural granularity required for UHR synthesis, and current diffusion training objectives do not incorporate spatial adaptivity into the denoising process. Together, these limitations present a core bottleneck for perceptually accurate ultra-high-resolution image generation.

In this work, we propose *Latent Wavelet Diffusion* (LWD), a general and modular framework that introduces frequency-sensitive spatial supervision into the latent denoising process of diffusion models. LWD is motivated by the observation that different regions of an image exhibit varying levels of structural complexity and perceptual importance. While some areas contain intricate textures or sharp edges, others are homogeneous or low in detail. Our goal is to exploit this spatial heterogeneity by allocating greater learning signal to regions with high visual complexity, and reducing supervision in low-detail areas. Importantly, LWD achieves this adaptivity without modifying the underlying architecture of the diffusion model, making it broadly applicable across model families.

The LWD framework consists of three key components:

1. A **spectrally-aware VAE fine-tuning objective** that improves the structure and diffusability of latent representations. By encouraging semantic consistency and frequency regularity, this objective enhances the suitability of latent spaces for high-resolution generation. It serves as the foundation for the subsequent components of LWD.
2. A **wavelet-derived spatial saliency map**, computed via a discrete wavelet transform (DWT) applied to the latent representation. This map aggregates the local energy of high-frequency subbands (LH, HL, HH) and is normalized to highlight spatial regions with strong structural detail. These saliency maps are interpretable, data-driven, and require no additional training, providing a principled measure of spatial importance directly from the signal.
3. A **time-dependent masking strategy** that leverages the frequency-based saliency maps to modulate the training loss. At each spatial location and timestep, a binary mask determines whether the denoising loss is applied. Regions with high wavelet energy receive supervision across more timesteps, while simpler areas are updated less frequently. This mechanism introduces spatial adaptivity into the learning process and improves the fidelity of fine-scale detail.

LWD is compatible with a broad range of latent diffusion models, including both classical diffusion and flow-matching formulations. Because it operates solely through the training objective, LWD can be seamlessly integrated into existing pipelines without requiring architectural changes or additional

inference cost. We demonstrate its flexibility and effectiveness by applying it to several state-of-the-art latent diffusion models and evaluating performance on ultra-high-resolution image synthesis (2K to 4K). Experimental results show that LWD consistently enhances perceptual quality, improves FID scores, and better preserves fine-grained detail, all without increasing inference complexity.

2 Related Work

Diffusion Models and Latent Generation. Diffusion models have become foundational in generative modeling, particularly for image synthesis [51, 70], by progressively denoising Gaussian noise using a learned score function. Variants based on stochastic differential equations [57], probability flow ordinary differential equations [34], and reinforcement-trained objectives [6] have expanded the design space with improved stability and sampling efficiency.

To reduce the cost of high-resolution generation, Latent Diffusion Models (LDMs) [47] perform synthesis in a compressed space learned via variational autoencoders (VAEs). However, generation quality is closely tied to the spectral fidelity and structure of these latent representations. Prior work has sought to improve this through enhanced VAE architectures [14], hierarchical compression [58], and frequency-aware regularization [55, 30]. We build on this direction by integrating frequency-sensitive supervision both during encoding and throughout the denoising process.

Flow Matching and High-Resolution Diffusion. Flow matching [34, 13] offers an alternative to classical diffusion by learning a continuous velocity field that maps noise to data in latent space, eliminating the need for fixed noise schedules. This formulation underlies models such as Flux [31], which, paired with DiT backbones, has demonstrated strong performance in ultra-high-resolution pipelines [71, 69]. Our method extends this family by introducing frequency-based spatial masking into the flow-matching objective. Through wavelet decomposition of the latent space, LWD computes spatial saliency maps that guide targeted supervision toward detail-rich regions, enhancing fine structure without modifying model architecture.

Variational Autoencoder Optimization. The performance of latent diffusion models at high resolutions depends critically on the expressiveness and spectral consistency of the VAE. Improvements include multi-scale encoders [60, 58], spectral loss functions [5], and scale-consistency constraints [55, 30]. Wavelet-based methods [15, 33, 1] enrich latent expressiveness by isolating frequency components, while compression-oriented approaches [65, 59, 18] aim to reduce token count for improved sampling efficiency. Our LWD fine-tunes a pretrained VAE with a scale-consistent spectral loss that suppresses spurious high-frequency noise. This regularized latent space facilitates downstream wavelet decomposition and supports our spatially adaptive denoising objective.

Ultra High-Resolution Image Synthesis. Maintaining global structure and fine detail in ultra-resolution generation is a persistent challenge. Standard diffusion models tend to produce repetitive patterns or distortions [20]. Existing solutions include cascaded generation [23], progressive up-sampling [16], domain-specific pipelines [46], and latent-space super-resolution [26]. However, training-based methods [66, 75, 17, 9] are resource-intensive, and training-free approaches [4, 32] often yield local artifacts.

Methods such as ScaleCrafter [20] mitigate repetition through dilated convolutions but may distort structure, while ResMaster [52] uses low-resolution references for guided refinement. HiDiffusion [73] introduces architectural changes that risk performance trade-offs, and progressive strategies like DemoFusion [11] suffer from slow inference and irregular patterns. Diffusion-4K [71] and URAE [69] advance latent modeling and parameter-efficient adaptation at 4K resolution. Our LWD complements these approaches by introducing signal-driven, spatially adaptive supervision that improves structural and perceptual fidelity for free.

Generative Modeling in the Frequency Domain. Frequency structure plays an increasingly important role in generative modeling [68]. Wavelet-based diffusion methods, such as WaveDiff [42], and spectral decomposition approaches have proven useful for efficient sampling [44], super-resolution [3, 53], and restoration [25, 74, 27]. FouriScale [24] demonstrated that frequency filtering enhances coherence, and DiffuseHigh [28] leveraged low-frequency DWT guidance to improve global structure in UHR synthesis.

Diffusion-4K [71] incorporated wavelet losses in the latent space to balance frequency bands, but applied them uniformly across all spatial locations. In contrast, LWD introduces wavelet-based

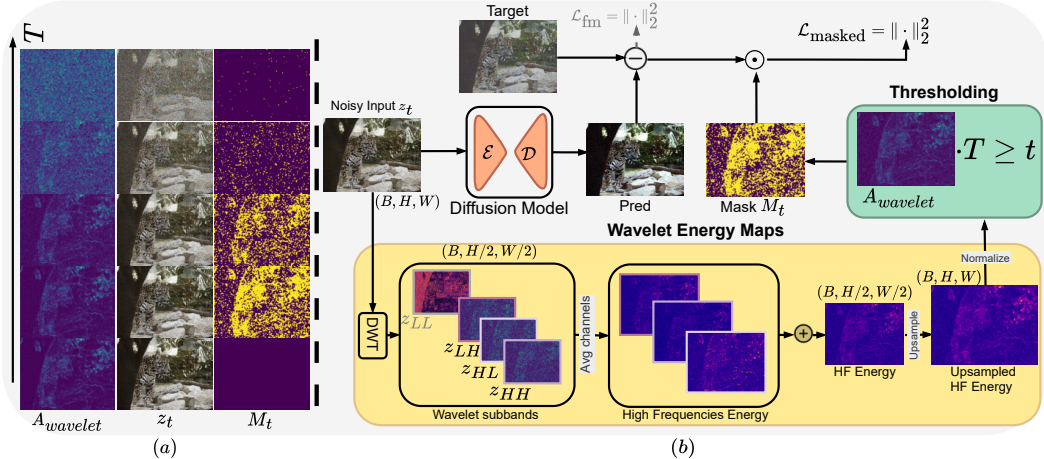


Figure 2: (a) Temporal evolution of latent z_t , wavelet energy maps $A_{wavelet}$, and attention map M_t across diffusion timesteps. (b) Our wavelet-masked flow matching objective at a timestep t . The model computes a wavelet attention map M_t from latent z_t to modulate the prediction error between target velocity field ($\epsilon - z_0$) and predicted velocity $v_{\Theta}(z_t, t, y)$. This focuses optimization on high-frequency regions with greater perceptual importance. While operations occur in latent space, decoded visualizations are shown for interpretability.

spatial conditioning through time-dependent masking. Rather than treating frequency as a passive loss signal, our LWD actively uses local frequency energy to modulate supervision across space and time, concentrating on learning where detail matters most. This enables sharper, more coherent synthesis without modifying the underlying model or increasing inference cost.

3 Methodology

Latent Wavelet Diffusion (LWD) introduces frequency-aware supervision into latent diffusion models by coupling signal-driven saliency analysis with adaptive training. Our key insight is that structural complexity in images is unevenly distributed in space, yet most denoising models refine all positions equally. LWD addresses this by modulating the supervision schedule based on local frequency content, improving detail fidelity without increasing computational cost.

LWD comprises two sequential stages. First, we fine-tune a variational autoencoder (VAE) using a scale-consistency objective to obtain spectrally stable and semantically meaningful latent representations. This step is performed independently and prepares the latent space for subsequent frequency-based modulation.

In the second stage, we fine-tune a latent diffusion model (e.g., Flux) using a modified flow-matching objective that integrates frequency-guided supervision. This stage incorporates three tightly coupled components: (1) extraction of wavelet-based spatial saliency maps from latent codes; (2) construction of a time-dependent mask that adapts the training signal based on local frequency energy; and (3) application of this mask to modulate the training loss dynamically across spatial positions and timesteps. Together, these mechanisms introduce spatial adaptivity into the denoising process, directing learning resources toward detail-rich regions. All components are model-agnostic and can be integrated into standard latent diffusion pipelines without architectural changes.

3.1 VAE Fine-Tuning with Scale-Consistency Loss

High-resolution generation places unique demands on the latent space: it must retain both semantic structure and spectral coherence across scales. To ensure this, we fine-tune the variational autoencoder (VAE) using a multi-resolution reconstruction objective that regularizes frequency content while preserving perceptual fidelity.

Formally, let $z = E(x)$ be the latent encoding of image x , x_{down} a downsampled version of x , and z_{down} the downsampled version of the latent z . Our loss combines four components:

$$\mathcal{L}_{\text{VAE}} = \underbrace{\|D(z) - x\|_2^2}_{\text{Reconstruction}} + \alpha \underbrace{\|D(E(z_{\text{down}})) - x_{\text{down}}\|_2^2}_{\text{Scale Consistency}} + \beta \underbrace{D_{\text{KL}}(q(z|x) \| p(z))}_{\text{Latent Regularization}} + \lambda \underbrace{\mathcal{L}_{\text{LPIPS}}(D(z), x)}_{\text{Perceptual Loss}}, \quad (1)$$

Here, we incorporate a scale-consistency term [55, 30] that encourages the VAE to maintain structural coherence across resolution scales. This regularization naturally suppresses high-frequency artifacts while ensuring robust encoding of essential structural information in z , which is critical for the downstream wavelet decomposition in LWD.

Unlike recent approaches that inject frequency conditioning directly into the encoder [3, 71], our formulation decouples signal regularization and generation: we first sculpt the latent space to exhibit desirable frequency properties, and then use this structure to guide the training of the diffusion model. This preserves architectural modularity while enabling effective frequency-aware supervision.

3.2 Wavelet-Derived Frequency Saliency Maps

To guide spatial supervision based on structural complexity, we extract saliency maps from latent representations using localized frequency analysis. Given a latent tensor $z \in \mathbb{R}^{C \times H \times W}$, we apply a single-level Discrete Wavelet Transform (DWT), producing four subbands:

$$\text{DWT}(z) \rightarrow \{z_{LL}, z_{LH}, z_{HL}, z_{HH}\}, \quad (2)$$

where z_{LL} captures low-frequency approximations and $\{z_{LH}, z_{HL}, z_{HH}\}$ encode directional high-frequency detail.

We compute the localized high-frequency energy as:

$$E(i, j) = \frac{1}{C} \sum_c \left[(z_{LH}^{c,i,j})^2 + (z_{HL}^{c,i,j})^2 + (z_{HH}^{c,i,j})^2 \right], \quad (3)$$

where (i, j) denotes spatial position and $c \in \{1, \dots, C\}$ indexes feature channels. The resulting energy map $E \in \mathbb{R}^{H/2 \times W/2}$ is bilinearly upsampled and min-max normalized per sample to obtain the final saliency map $A_{\text{wavelet}} \in [0, 1]^{H \times W}$.

This map serves as a proxy for local structural richness, highlighting regions of the latent space associated with high-frequency content (e.g., textures, contours, transitions). Unlike learned attention mechanisms based on semantic similarity (e.g., DINO [8]), our approach is deterministic and directly derived from signal properties. While we refer to A_{wavelet} as an "attention map" for interpretability, it is best understood as a frequency-aware saliency measure.

Notably, our VAE fine-tuning objective (Eq. 1) helps suppress high-frequency artifacts and stabilize spectral behavior. This preprocessing step ensures that high-frequency activations captured by the DWT correspond to meaningful structure, rather than encoding noise, thereby improving the utility of A_{wavelet} for guiding spatial supervision.

3.3 Adaptive Flow Matching with Frequency-Guided Masking

We adopt a continuous-time flow-matching formulation [34, 13] for training the latent diffusion model. Given a target latent z_0 and noise sample $\epsilon \sim \mathcal{N}(0, I)$, we define interpolated samples as:

$$z_t = (1 - t)z_0 + t\epsilon, \quad t \in [0, 1], \quad (4)$$

and supervise the predicted velocity field $v_{\ominus}(z_t, t, y)$, conditioned on text y , via:

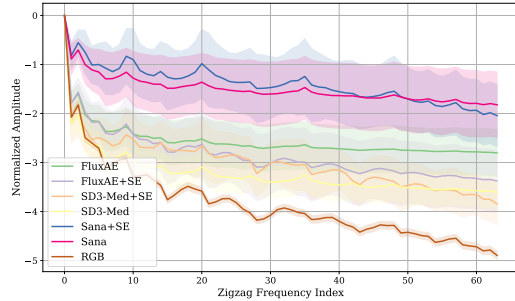


Figure 3: Normalized DCT amplitudes over zigzag frequency indices. VAE trained with the multi-scale loss reduces high-frequency energy in latents, aligning their spectrum with that of RGB images.

$$\mathcal{L}_{\text{fm}} = \|(\epsilon - z_0) - v_{\Theta}(z_t, t, y)\|_2^2. \quad (5)$$

To incorporate frequency-awareness into the training objective, we apply spatially adaptive masking based on the wavelet saliency map A_{wavelet} . Specifically, for each location (i, j) , we define a time-dependent binary mask:

$$M_t(i, j) = \begin{cases} 1 & \text{if } T \cdot (A_{\text{wavelet}}(i, j) + \ell) \geq t \\ 0 & \text{otherwise} \end{cases}, \quad (6)$$

where T is the total number of training steps and $\ell \in (0, 1)$ sets a lower bound on refinement. This ensures that all regions receive at least ℓT steps of supervision, while high-frequency regions benefit from extended refinement.

While selective spatial supervision has been investigated using transformer attention [40], our wavelet-derived saliency offers a fundamentally different perspective based on signal processing principles rather than learned semantic features, offering computational advantages and a more generalizable solution.

The final masked loss becomes:

$$\mathcal{L}_{\text{masked}} = \|M_t \odot [(\epsilon - z_0) - v_{\Theta}(z_t, t, y)]\|_2^2, \quad (7)$$

where \odot denotes element-wise multiplication. This formulation focuses learning capacity on detail-rich regions, improves fidelity in high-frequency content, and does so without increasing inference complexity. Crucially, this mechanism operates purely at the objective level and is compatible with any latent diffusion model using a flow-based or score-based trajectory.

4 Experiments

4.1 Experimental Setup

Datasets. We evaluate LWD on two ultra-resolution datasets. Aesthetic-4K [71] is a curated 4K benchmark with GPT-4o-generated captions and high visual quality. LAION-High-Res is a filtered subset of LAION-5B [50], from which we sample 50K 2K-resolution and 20K 4K-resolution image-caption pairs. These two datasets differ in both visual and linguistic distributions, allowing us to assess both generation fidelity and generalization under caption variance.

Implementation Details. We implement LWD using PyTorch and `pytorch-wavelets` [10] for Haar-based DWT. VAE fine-tuning is performed for 60K steps with a batch size of 4 and a learning rate of 1×10^{-5} on NVIDIA A100 GPUs. The frequency-guided loss is applied during the training of the architectures we tested. We set the masking lower bound $\ell = 0.3$, selected via ablation to ensure each spatial location receives at least 30% of refinement steps. We will release the code on GitHub after the review process. Training requirements varied across architectures. LWD+URAE (Flux-based) [31, 69] required approximately 4 hours and 2k iterations at batch size 1 for the 2048 version, while the 4096 version needed 24 hours for 2k iterations, significantly fewer than the original work, which suggests 10k iterations. Diffusion4K (SD3-based) [13, 71] was trained for 48 hours at 10k iterations (half the originally required iterations) with batch size 8 for the 2048 version, maintaining identical parameters for the 4096 version except with batch size 4. SANA [65] models (both 2048 and 4096 versions) were trained for 24 hours, achieving 33k iterations (one-third of the originally suggested iterations) with batch sizes of 2 and 1, respectively. PixArt- Σ [9] required only 24 hours and 1.5k iterations at batch size 2, compared to the suggested 15k iterations.

Evaluation Metrics. To comprehensively evaluate ultra-resolution text-to-image generation, we report multiple complementary metrics across three dimensions: image quality (Fréchet Inception Distance (FID), LPIPS), semantic alignment (CLIPScore [21], QualiCLIP [2]), and perceptual quality (MAN-IQA [67], HPSv2.1 [64], PickScore [29]). Note that lower values indicate better performance for FID and LPIPS, while higher values are preferred for all other metrics. We assess texture fidelity with the Gray Level Co-occurrence Matrix (GLCM) Score [71] and fine-grained detail preservation using JPEG Compression Ratio to measure high-frequency compressibility as a perceptual quality proxy.



Figure 4: Visual comparison of 2K image generations. LWD demonstrates improved detail preservation in complex areas while avoiding over-sharpening or texture collapse.

Table 1: Quantitative results on different metrics. The prompts are from the HPD [64] dataset. All images are at a resolution of 2048×2048 .

| Model | FID ↓ | LPIPS ↓ | MAN-IQA ↑ | QualiCLIP ↑ | HPSv2.1 ↑ | PickScore ↑ |
|-----------------------|--------------|---------------|---------------|---------------|--------------|--------------|
| SDEdit [39] | 35.59 | 0.6456 | 0.3736 | 0.4480 | <u>30.92</u> | 22.86 |
| I-Max [12] | 36.28 | 0.6750 | 0.3641 | 0.4139 | 30.62 | 23.02 |
| PixArt-Sigma-XL [9] | 36.58 | 0.6801 | 0.2949 | 0.4438 | 30.66 | <u>22.92</u> |
| Sana-1.6B [65] | 35.75 | 0.7169 | 0.3666 | 0.5796 | <u>30.42</u> | 22.83 |
| Lumina-Image 2.0 [45] | 54.96 | 0.6445 | 0.3663 | 0.4567 | 23.08 | 21.15 |
| FLUX-1.dev [31] | 37.58 | <u>0.6371</u> | 0.4110 | 0.5468 | 28.73 | 22.68 |
| URAE [69] | <u>35.25</u> | 0.6717 | 0.4076 | <u>0.5423</u> | 31.15 | 22.41 |
| LWD + URAE | 32.88 | 0.6336 | <u>0.4099</u> | 0.5356 | 28.78 | 22.43 |

4.2 Quantitative Results

2K Results. Table 1 and the top block of Table 2 demonstrate consistent improvements from integrating LWD across multiple backbone models. On the HPD prompt dataset [64], LWD reduces FID by up to 7% and LPIPS up to 6% while also achieving comparable MAN-IQA and QualiCLIP, indicating improved semantic alignment and perceptual quality. Moreover, on the Aesthetic dataset [71], these gains are observed across diverse architectures, reinforcing the generality and model-agnostic nature of our approach.

4K Results. On the Aesthetic-4K (the bottom block of Table 2) and HPD prompt dataset [64] (can be found in the supplementary materials), LWD outperforms baselines such as URAE and PixArt-Sigma, particularly in metrics like FID, CLIPScore and Aesthetics. The improvements are especially pronounced in regions with fine structural detail, such as hair, foliage, or architectural elements, highlighting LWD’s ability to scale effectively to ultra-high resolutions. These results suggest that frequency-aware supervision provides meaningful guidance even in challenging high-frequency regimes where baseline methods often struggle. LWD also achieves the highest GLCM score when paired with SD3-F16, and substantially improves Sana’s performance on both GLCM and compression ratio, indicating stronger fine-detail retention and texture fidelity, without compromising overall quality.

Table 2: Quantitative benchmarks of latent diffusion models on Aesthetic-Eval at 2048×2048 and 4096×4096 . GLCM Score measures high-frequency texture richness using gray-level co-occurrence matrices, while Compression Ratio assesses visual complexity via JPEG file size heuristics, both introduced in Diffusion-4K [71].

| | Model | FID ↓ | CLIPScore ↑ | Aesthetics ↑ | GLCM Score ↑ | Compression Ratio ↓ |
|-----------------|-----------------------|--------------|--------------|--------------|--------------|---------------------|
| 2K | SD3-F16 [13] | 43.82 | 31.50 | 5.91 | 0.75 | 11.23 |
| | SD3-Diff4k-F16 [71] | 40.18 | 34.04 | 5.96 | 0.79 | 11.73 |
| | LWD + SD3-F16 | 38.74 | 34.94 | 6.17 | 0.74 | 11.99 |
| | PixArt-Sigma-XL [9] | 39.13 | 35.02 | 6.43 | 0.79 | 13.66 |
| | LWD + PixArt-Sigma-XL | 36.14 | 35.21 | 6.27 | 0.87 | 6.05 |
| | Sana-1.6B [65] | 32.06 | 35.28 | 6.15 | 0.93 | 24.01 |
| LWD + Sana-1.6B | 34.30 | 35.58 | 6.23 | 0.78 | 27.34 | |
| 4K | SD3-F16 [13] | - | 33.12 | 5.97 | 0.73 | 11.97 |
| | SD3-Diff4k-F16 [71] | - | 33.41 | 5.97 | 0.70 | 11.90 |
| | LWD + SD3-F16 | - | 34.08 | 6.03 | 0.77 | 12.27 |
| | Sana-1.6B [65] | - | 34.40 | 6.14 | 0.39 | 48.36 |
| | LWD + Sana-1.6B | - | 34.59 | 6.21 | 0.60 | 32.62 |

4.3 Qualitative Results

Figures 4, 5, and 9 compare outputs from LWD and baseline models under identical prompts. LWD consistently renders sharper textures in high-frequency regions, such as fabric, skin, and hair, while preserving global structure.

Zoomed-in comparisons highlight improved reconstruction of fine details (e.g., hair strands, eyelashes, small objects) that are often blurred or omitted by baselines. These results suggest that frequency-aware masking not only enhances local precision but does so in a context-sensitive manner, avoiding over-sharpening or artifacts. This indicates that LWD effectively balances fine detail refinement with structural coherence. More full-resolution results can be found in Appendix C and supplementary materials.

4.4 Discussion

Across quantitative and qualitative benchmarks, LWD enhances ultra-resolution image synthesis by integrating signal-derived saliency into the training loss. Compared to both conventional models and prior wavelet-based methods (e.g., Diffusion-4K), it improves perceptual fidelity, semantic alignment, and spectral regularity, without increasing inference cost or modifying the underlying architecture. Its plug-and-play nature makes it broadly compatible with modern latent diffusion pipelines.

Beyond quality gains, LWD represents a shift toward more interpretable and structure-aware supervision. Unlike attention mechanisms that rely on semantic priors, LWD leverages wavelet energy as a transparent, self-supervised signal to prioritize detail-rich regions.

This frequency-guided supervision introduces a form of spatial curriculum learning, where complex regions receive more focused updates. Such adaptive loss weighting opens avenues for dynamic training strategies, such as frequency-aware learning rates or hybrid spatial-frequency schedules. These mechanisms may be especially valuable in domains where structural detail is critical but semantic guidance is weak, such as scientific visualization, material design, or multimodal generation.

Limitations and Future Work. While LWD improves generation quality without architectural changes or inference overhead, it inherits certain limitations common to latent diffusion models. In particular, the compression imposed by the VAE can result in the loss of fine-grained semantic detail, potentially limiting performance in tasks that require precise spatial alignment or photorealistic accuracy.

Future work could address this by incorporating higher-fidelity latent spaces or hybrid approaches that combine latent and pixel-space supervision. Extending LWD to domains such as video generation, depth-aware synthesis, or multimodal conditioning also represents a promising direction. The frequency-aware masking mechanism is general and could be adapted to guide temporal attention, cross-modal alignment, or resolution-specific sampling in broader generative contexts.

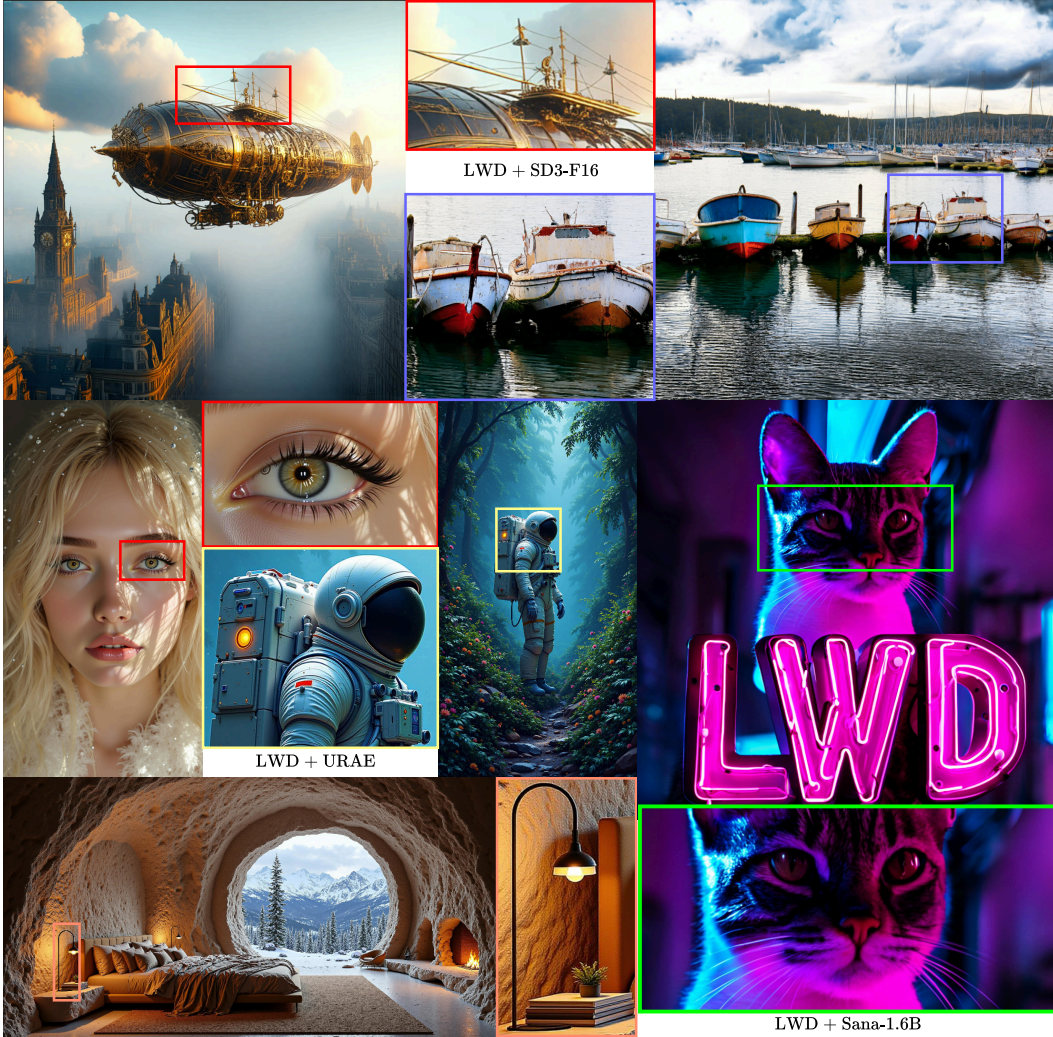


Figure 5: 4K images generated by LWD with different architectures.

5 Conclusion

We introduced *Latent Wavelet Diffusion* (LWD), a general and modular framework that integrates frequency-based supervision into latent diffusion models for ultra-high-resolution image synthesis. By computing wavelet energy maps in the latent space and applying spatially and temporally adaptive masking, LWD selectively emphasizes high-detail regions during training. Without requiring architectural modifications or incurring additional inference cost, LWD consistently improves perceptual fidelity and semantic alignment across models such as Flux and SD3. It preserves high-frequency detail and structural coherence more effectively than prior methods, demonstrating the value of signal-aware supervision in guiding the generative process. By unifying principles from signal processing and diffusion modeling, LWD offers a scalable and interpretable approach applicable to a wide range of generative architectures.

Broader Impact. LWD promotes efficient and interpretable generation by aligning supervision with signal-level detail. This may benefit applications requiring controllable high-resolution synthesis, while raising familiar concerns around synthetic media misuse. Incorporating safeguards and provenance tools remains an important direction.

References

- [1] Niket Agarwal, Arslan Ali, Maciej Bala, Yogesh Balaji, Erik Barker, Tiffany Cai, Prithvijit Chattopadhyay, Yongxin Chen, Yin Cui, Yifan Ding, et al. Cosmos world foundation model platform for physical ai. *arXiv preprint arXiv:2501.03575*, 2025.
- [2] Lorenzo Agnolucci, Leonardo Galteri, and Marco Bertini. Quality-aware image-text alignment for opinion-unaware image quality assessment. *arXiv preprint arXiv:2403.11176*, 2024.
- [3] Lorenzo Aloisi, Luigi Sigillo, Aurelio Uncini, and Danilo Comminiello. A wavelet diffusion gan for image super-resolution. *arXiv preprint arXiv:2410.17966*, 2024.
- [4] Omer Bar-Tal, Lior Yariv, Yaron Lipman, and Tali Dekel. MultiDiffusion: Fusing diffusion paths for controlled image generation. In Andreas Krause, Emma Brunskill, Kyunghyun Cho, Barbara Engelhardt, Sivan Sabato, and Jonathan Scarlett, editors, *Proceedings of the 40th International Conference on Machine Learning*, volume 202 of *Proceedings of Machine Learning Research*, pages 1737–1752. PMLR, 23–29 Jul 2023.
- [5] Sara Björk, Jonas Nordhaug Myhre, and Thomas Haugland Johansen. Simpler is better: Spectral regularization and up-sampling techniques for variational autoencoders. In *ICASSP 2022 - 2022 IEEE International Conference on Acoustics, Speech and Signal Processing (ICASSP)*, pages 3778–3782, 2022.
- [6] Kevin Black, Michael Janner, Yilun Du, Ilya Kostrikov, and Sergey Levine. Training diffusion models with reinforcement learning. In *The Twelfth International Conference on Learning Representations*, 2024.
- [7] Tim Brooks, Aleksander Holynski, and Alexei A Efros. Instructpix2pix: Learning to follow image editing instructions. In *Proceedings of the IEEE/CVF conference on computer vision and pattern recognition*, pages 18392–18402, 2023.
- [8] Mathilde Caron, Hugo Touvron, Ishan Misra, Hervé Jégou, Julien Mairal, Piotr Bojanowski, and Armand Joulin. Emerging properties in self-supervised vision transformers. In *Proceedings of the IEEE/CVF international conference on computer vision*, pages 9650–9660, 2021.
- [9] Junsong Chen, Chongjian Ge, Enze Xie, Yue Wu, Lewei Yao, Xiaozhe Ren, Zhongdao Wang, Ping Luo, Huchuan Lu, and Zhenguo Li. Pixart- σ : Weak-to-strong training of diffusion transformer for 4k text-to-image generation. In *European Conference on Computer Vision*, pages 74–91. Springer, 2024.
- [10] Fergal Cotter. *Uses of Complex Wavelets in Deep Convolutional Neural Networks*. PhD thesis, Apollo - University of Cambridge Repository, 2019.
- [11] Ruoyi Du, Dongliang Chang, Timothy Hospedales, Yi-Zhe Song, and Zhanyu Ma. Demofusion: Democratising high-resolution image generation with no \$\$\$\$. In *Proceedings of the IEEE/CVF Conference on Computer Vision and Pattern Recognition*, pages 6159–6168, 2024.
- [12] Ruoyi Du, Dongyang Liu, Le Zhuo, Qin Qi, Hongsheng Li, Zhanyu Ma, and Peng Gao. I-max: Maximize the resolution potential of pre-trained rectified flow transformers with projected flow, 2024.
- [13] Patrick Esser, Sumith Kulal, Andreas Blattmann, Rahim Entezari, Jonas Müller, Harry Saini, Yam Levi, Dominik Lorenz, Axel Sauer, Frederic Boesel, et al. Scaling rectified flow transformers for high-resolution image synthesis. In *Forty-first international conference on machine learning*, 2024.
- [14] Patrick Esser, Robin Rombach, and Bjorn Ommer. Taming transformers for high-resolution image synthesis. In *Proceedings of the IEEE/CVF conference on computer vision and pattern recognition*, pages 12873–12883, 2021.
- [15] Carlos Esteves, Mohammed Suhail, and Ameesh Makadia. Spectral image tokenizer. *arXiv preprint arXiv:2412.09607*, 2024.

- [16] Jiatao Gu, Shuangfei Zhai, Yizhe Zhang, Joshua M. Susskind, and Navdeep Jaitly. Matryoshka diffusion models. In *The Twelfth International Conference on Learning Representations*, 2024.
- [17] Lanqing Guo, Yingqing He, Haoxin Chen, Menghan Xia, Xiaodong Cun, Yufei Wang, Siyu Huang, Yong Zhang, Xintao Wang, Qifeng Chen, et al. Make a cheap scaling: A self-cascade diffusion model for higher-resolution adaptation. In *European Conference on Computer Vision*, pages 39–55. Springer, 2024.
- [18] Yoav HaCohen, Nisan Chiprut, Benny Brazowski, Daniel Shalem, Dudu Moshe, Eitan Richardson, Eran Levin, Guy Shiran, Nir Zabari, Ori Gordon, et al. Ltx-video: Realtime video latent diffusion. *arXiv preprint arXiv:2501.00103*, 2024.
- [19] Jaehoon Hahm, Junho Lee, Sunghyun Kim, and Joonseok Lee. Isometric representation learning for disentangled latent space of diffusion models. In *Forty-first International Conference on Machine Learning*, 2024.
- [20] Yingqing He, Shaoshu Yang, Haoxin Chen, Xiaodong Cun, Menghan Xia, Yong Zhang, Xintao Wang, Ran He, Qifeng Chen, and Ying Shan. Scalecrafter: Tuning-free higher-resolution visual generation with diffusion models. In *The Twelfth International Conference on Learning Representations*, 2023.
- [21] Jack Hessel, Ari Holtzman, Maxwell Forbes, Ronan Le Bras, and Yejin Choi. Clipscore: A reference-free evaluation metric for image captioning. In *EMNLP (1)*, 2021.
- [22] Jonathan Ho, Ajay Jain, and Pieter Abbeel. Denoising diffusion probabilistic models. *Advances in neural information processing systems*, 33:6840–6851, 2020.
- [23] Jonathan Ho, Chitwan Saharia, William Chan, David J Fleet, Mohammad Norouzi, and Tim Salimans. Cascaded diffusion models for high fidelity image generation. *Journal of Machine Learning Research*, 23(47):1–33, 2022.
- [24] Linjiang Huang, Rongyao Fang, Aiping Zhang, Guanglu Song, Si Liu, Yu Liu, and Hongsheng Li. Fouriscale: A frequency perspective on training-free high-resolution image synthesis. In *European Conference on Computer Vision*, pages 196–212. Springer, 2024.
- [25] Yi Huang, Jiancheng Huang, Jianzhuang Liu, Mingfu Yan, Yu Dong, Jiayi Lv, Chaoqi Chen, and Shifeng Chen. Wavedm: Wavelet-based diffusion models for image restoration. *IEEE Transactions on Multimedia*, 26:7058–7073, 2024.
- [26] Jinho Jeong, Sangmin Han, Jinwoo Kim, and Seon Joo Kim. Latent space super-resolution for higher-resolution image generation with diffusion models. *arXiv preprint arXiv:2503.18446*, 2025.
- [27] Hai Jiang, Ao Luo, Haoqiang Fan, Songchen Han, and Shuaicheng Liu. Low-light image enhancement with wavelet-based diffusion models. *ACM Trans. Graph.*, 42(6), December 2023.
- [28] Youngyun Kim, Geunmin Hwang, Junyu Zhang, and Eunbyung Park. Diffusehigh: Training-free progressive high-resolution image synthesis through structure guidance. In *Proceedings of the AAAI conference on artificial intelligence*, volume 39, pages 4338–4346, 2025.
- [29] Yuval Kirstain, Adam Polyak, Uriel Singer, Shahbuland Matiana, Joe Penna, and Omer Levy. Pick-a-pic: An open dataset of user preferences for text-to-image generation. *Advances in Neural Information Processing Systems*, 36:36652–36663, 2023.
- [30] Theodoros Kouzelis, Ioannis Kakogeorgiou, Spyros Gidaris, and Nikos Komodakis. Eq-vae: Equivariance regularized latent space for improved generative image modeling. *arXiv preprint arXiv:2502.09509*, 2025.
- [31] Black Forest Labs. Flux. <https://github.com/black-forest-labs/flux>, 2024.
- [32] Yuseung Lee, Kunho Kim, Hyunjin Kim, and Minhyuk Sung. Syncdiffusion: Coherent montage via synchronized joint diffusions. *Advances in Neural Information Processing Systems*, 36:50648–50660, 2023.

- [33] Bin Lin, Yunyang Ge, Xinhua Cheng, Zongjian Li, Bin Zhu, Shaodong Wang, Xianyi He, Yang Ye, Shenghai Yuan, Liuhan Chen, et al. Open-sora plan: Open-source large video generation model. *arXiv preprint arXiv:2412.00131*, 2024.
- [34] Yaron Lipman, Ricky T. Q. Chen, Heli Ben-Hamu, Maximilian Nickel, and Matthew Le. Flow matching for generative modeling. In *The Eleventh International Conference on Learning Representations*, 2023.
- [35] Guangyi Liu, Yu Wang, Zeyu Feng, Qiyu Wu, Liping Tang, Yuan Gao, Zhen Li, Shuguang Cui, Julian McAuley, Zichao Yang, Eric P. Xing, and Zhiting Hu. Unified generation, reconstruction, and representation: Generalized diffusion with adaptive latent encoding-decoding. In *Forty-first International Conference on Machine Learning*, 2024.
- [36] Yixin Liu, Kai Zhang, Yuan Li, Zhiling Yan, Chujie Gao, Ruoxi Chen, Zhengqing Yuan, Yue Huang, Hanchi Sun, Jianfeng Gao, Lifang He, and Lichao Sun. Sora: A review on background, technology, limitations, and opportunities of large vision models, 2024.
- [37] Eleonora Lopez, Luigi Sigillo, Federica Colonnese, Massimo Panella, and Danilo Comminiello. Guess what i think: Streamlined eeg-to-image generation with latent diffusion models. In *ICASSP 2025 - 2025 IEEE International Conference on Acoustics, Speech and Signal Processing (ICASSP)*, pages 1–5, 2025.
- [38] Stephane Mallat and Wen Liang Hwang. Singularity detection and processing with wavelets. *IEEE transactions on information theory*, 38(2):617–643, 1992.
- [39] Chenlin Meng, Yutong He, Yang Song, Jiaming Song, Jiajun Wu, Jun-Yan Zhu, and Stefano Ermon. SDEdit: Guided image synthesis and editing with stochastic differential equations. In *International Conference on Learning Representations*, 2022.
- [40] Brian B. Moser, Stanislav Frolov, Federico Raue, Sebastian Palacio, and Andreas Dengel. Dynamic Attention-Guided Diffusion for Image Super-Resolution . In *2025 IEEE/CVF Winter Conference on Applications of Computer Vision (WACV)*, pages 451–460, Los Alamitos, CA, USA, March 2025. IEEE Computer Society.
- [41] William Peebles and Saining Xie. Scalable diffusion models with transformers. In *Proceedings of the IEEE/CVF international conference on computer vision*, pages 4195–4205, 2023.
- [42] Hao Phung, Quan Dao, and Anh Tran. Wavelet diffusion models are fast and scalable image generators. In *Proceedings of the IEEE/CVF conference on computer vision and pattern recognition*, pages 10199–10208, 2023.
- [43] Dustin Podell, Zion English, Kyle Lacey, Andreas Blattmann, Tim Dockhorn, Jonas Müller, Joe Penna, and Robin Rombach. SDXL: Improving latent diffusion models for high-resolution image synthesis. In *The Twelfth International Conference on Learning Representations*, 2024.
- [44] Yurui Qian, Qi Cai, Yingwei Pan, Yehao Li, Ting Yao, Qibin Sun, and Tao Mei. Boosting diffusion models with moving average sampling in frequency domain. In *Proceedings of the IEEE/CVF Conference on Computer Vision and Pattern Recognition*, pages 8911–8920, 2024.
- [45] Qi Qin, Le Zhuo, Yi Xin, Ruoyi Du, Zhen Li, Bin Fu, Yiting Lu, Jiakang Yuan, Xinyue Li, Dongyang Liu, et al. Lumina-image 2.0: A unified and efficient image generative framework. *arXiv preprint arXiv:2503.21758*, 2025.
- [46] Jingjing Ren, Wenbo Li, Haoyu Chen, Renjing Pei, Bin Shao, Yong Guo, Long Peng, Fenglong Song, and Lei Zhu. Ultrapixel: Advancing ultra high-resolution image synthesis to new peaks. In *The Thirty-eighth Annual Conference on Neural Information Processing Systems*, 2024.
- [47] Robin Rombach, Andreas Blattmann, Dominik Lorenz, Patrick Esser, and Björn Ommer. High-resolution image synthesis with latent diffusion models. In *Proceedings of the IEEE/CVF conference on computer vision and pattern recognition*, pages 10684–10695, 2022.
- [48] Chitwan Saharia, Jonathan Ho, William Chan, Tim Salimans, David J Fleet, and Mohammad Norouzi. Image super-resolution via iterative refinement. *IEEE transactions on pattern analysis and machine intelligence*, 45(4):4713–4726, 2022.

- [49] Axel Sauer, Dominik Lorenz, Andreas Blattmann, and Robin Rombach. Adversarial diffusion distillation. In *European Conference on Computer Vision*, pages 87–103. Springer, 2024.
- [50] Christoph Schuhmann, Romain Beaumont, Richard Vencu, Cade Gordon, Ross Wightman, Mehdi Cherti, Theo Coombes, Aarush Katta, Clayton Mullis, Mitchell Wortsman, Patrick Schramowski, Srivatsa Kundurthy, Katherine Crowson, Ludwig Schmidt, Robert Kaczmarczyk, and Jenia Jitsev. Laion-5b: an open large-scale dataset for training next generation image-text models. In *Proceedings of the 36th International Conference on Neural Information Processing Systems*, NIPS '22, Red Hook, NY, USA, 2022. Curran Associates Inc.
- [51] Hui Shen, Jingxuan Zhang, Boning Xiong, Rui Hu, Shoufa Chen, Zhongwei Wan, Xin Wang, Yu Zhang, Zixuan Gong, Guanyin Bao, Chaofan Tao, Yongfeng Huang, Ye Yuan, and Mi Zhang. Efficient diffusion models: A survey. *Transactions on Machine Learning Research*, 2025.
- [52] Shuwei Shi, Wenbo Li, Yuechen Zhang, Jingwen He, Biao Gong, and Yinqiang Zheng. Resmaster: Mastering high-resolution image generation via structural and fine-grained guidance. In *Proceedings of the AAAI Conference on Artificial Intelligence*, volume 39, pages 6887–6895, 2025.
- [53] Luigi Sigillo, Christian Bianchi, Aurelio Uncini, and Danilo Comminiello. Quaternion wavelet-conditioned diffusion models for image super-resolution. In *2025 International Joint Conference on Neural Networks (IJCNN)*, pages 1–8, 2025.
- [54] Luigi Sigillo, Riccardo Fosco Gramaccioni, Alessandro Nicolosi, and Danilo Comminiello. Ship in sight: Diffusion models for ship-image super resolution. In *2024 International Joint Conference on Neural Networks (IJCNN)*, pages 1–8, 2024.
- [55] Ivan Skorokhodov, Sharath Girish, Benran Hu, Willi Menapace, Yanyu Li, Rameen Abdal, Sergey Tulyakov, and Aliaksandr Siarohin. Improving the diffusability of autoencoders, 2025.
- [56] Jiaming Song, Chenlin Meng, and Stefano Ermon. Denoising diffusion implicit models. In *International Conference on Learning Representations*, 2021.
- [57] Yang Song, Jascha Sohl-Dickstein, Diederik P Kingma, Abhishek Kumar, Stefano Ermon, and Ben Poole. Score-based generative modeling through stochastic differential equations. In *International Conference on Learning Representations*, 2021.
- [58] Yuhta Takida, Yukara Ikemiya, Takashi Shibuya, Kazuki Shimada, Woosung Choi, Chieh-Hsin Lai, Naoki Murata, Toshimitsu Uesaka, Kengo Uchida, Wei-Hsiang Liao, and Yuki Mitsufuji. HQ-VAE: Hierarchical discrete representation learning with variational bayes. *Transactions on Machine Learning Research*, 2024.
- [59] Anni Tang, Tianyu He, Junliang Guo, Xinle Cheng, Li Song, and Jiang Bian. Vidtok: A versatile and open-source video tokenizer. *arXiv preprint arXiv:2412.13061*, 2024.
- [60] Arash Vahdat and Jan Kautz. Nvae: A deep hierarchical variational autoencoder. *Advances in neural information processing systems*, 33:19667–19679, 2020.
- [61] Yufei Wang, Wenhan Yang, Xinyuan Chen, Yaohui Wang, Lanqing Guo, Lap-Pui Chau, Ziwei Liu, Yu Qiao, Alex C Kot, and Bihan Wen. Sinsr: diffusion-based image super-resolution in a single step. In *Proceedings of the IEEE/CVF Conference on Computer Vision and Pattern Recognition*, pages 25796–25805, 2024.
- [62] Z. Wang, E.P. Simoncelli, and A.C. Bovik. Multiscale structural similarity for image quality assessment. In *The Thirty-Seventh Asilomar Conference on Signals, Systems & Computers, 2003*, volume 2, pages 1398–1402 Vol.2, 2003.
- [63] Zhendong Wang, Jianmin Bao, Shuyang Gu, Dong Chen, Wengang Zhou, and Houqiang Li. Designdiffusion: High-quality text-to-design image generation with diffusion models, 2025.
- [64] Xiaoshi Wu, Yiming Hao, Keqiang Sun, Yixiong Chen, Feng Zhu, Rui Zhao, and Hongsheng Li. Human preference score v2: A solid benchmark for evaluating human preferences of text-to-image synthesis, 2023.

- [65] Enze Xie, Junsong Chen, Junyu Chen, Han Cai, Haotian Tang, Yujun Lin, Zhekai Zhang, Muyang Li, Ligeng Zhu, Yao Lu, and Song Han. SANA: Efficient high-resolution text-to-image synthesis with linear diffusion transformers. In *The Thirteenth International Conference on Learning Representations*, 2025.
- [66] Enze Xie, Lewei Yao, Han Shi, Zhili Liu, Daquan Zhou, Zhaoqiang Liu, Jiawei Li, and Zhenguo Li. Diffit: Unlocking transferability of large diffusion models via simple parameter-efficient fine-tuning. In *Proceedings of the IEEE/CVF International Conference on Computer Vision*, pages 4230–4239, 2023.
- [67] Sidi Yang, Tianhe Wu, Shuwei Shi, Shanshan Lao, Yuan Gong, Mingdeng Cao, Jiahao Wang, and Yujiu Yang. Maniqa: Multi-dimension attention network for no-reference image quality assessment. In *Proceedings of the IEEE/CVF conference on computer vision and pattern recognition*, pages 1191–1200, 2022.
- [68] Xingyi Yang, Daquan Zhou, Jiashi Feng, and Xinchao Wang. Diffusion probabilistic model made slim. In *2023 IEEE/CVF Conference on Computer Vision and Pattern Recognition (CVPR)*, pages 22552–22562, 2023.
- [69] Ruonan Yu, Songhua Liu, Zhenxiong Tan, and Xinchao Wang. Ultra-resolution adaptation with ease. *International Conference on Machine Learning*, 2025.
- [70] Zheyuan Zhan, Defang Chen, Jian-Ping Mei, Zhenghe Zhao, Jiawei Chen, Chun Chen, Siwei Lyu, and Can Wang. Conditional image synthesis with diffusion models: A survey. *CoRR*, abs/2409.19365, 2024.
- [71] Jinjin Zhang, Qiuyu Huang, Junjie Liu, Xiefan Guo, and Di Huang. Diffusion-4k: Ultra-high-resolution image synthesis with latent diffusion models. In *IEEE/CVF Conference on Computer Vision and Pattern Recognition (CVPR)*, 2025.
- [72] Lin Zhang, Lei Zhang, Xuanqin Mou, and David Zhang. Fsim: A feature similarity index for image quality assessment. *IEEE Transactions on Image Processing*, 20(8):2378–2386, 2011.
- [73] Lvmin Zhang, Anyi Rao, and Maneesh Agrawala. Adding conditional control to text-to-image diffusion models. In *Proceedings of the IEEE/CVF international conference on computer vision*, pages 3836–3847, 2023.
- [74] Chen Zhao, Weiling Cai, Chenyu Dong, and Chengwei Hu. Wavelet-based fourier information interaction with frequency diffusion adjustment for underwater image restoration. In *Proceedings of the IEEE/CVF Conference on Computer Vision and Pattern Recognition*, pages 8281–8291, 2024.
- [75] Qingping Zheng, Yuanfan Guo, Jiankang Deng, Jianhua Han, Ying Li, Songcen Xu, and Hang Xu. Any-size-diffusion: Toward efficient text-driven synthesis for any-size hd images. In *Proceedings of the AAAI Conference on Artificial Intelligence*, volume 38, pages 7571–7578, 2024.

A Wavelet-Based Relevance Maps for Latent Space Analysis

A.1 Discrete Wavelet Transform (DWT)

The Discrete Wavelet Transform (DWT) decomposes a 2D signal, such as an image or a latent tensor, into orthogonal frequency subbands by applying separable cascades of low-pass and high-pass filters along both spatial dimensions. Given an input $\mathbf{X} \in \mathbb{R}^{H \times W \times D}$, a single-level DWT produces four spatial subbands:

- **LL** (Low-Low): Approximation coefficients capturing global structure and coarse semantics.
- **LH** (Low-High): Horizontal detail coefficients, sensitive to vertical edges.
- **HL** (High-Low): Vertical detail coefficients, highlighting horizontal edges.
- **HH** (High-High): Diagonal detail coefficients, encoding fine textures and high-frequency transitions.

Formally, the DWT of \mathbf{X} is given by:

$$\text{DWT}(\mathbf{X}) = \begin{cases} \text{LL} = \mathbf{X} * h_{\text{low}} \downarrow 2 * h_{\text{low}} \downarrow 2 \\ \text{LH} = \mathbf{X} * h_{\text{low}} \downarrow 2 * h_{\text{high}} \downarrow 2 \\ \text{HL} = \mathbf{X} * h_{\text{high}} \downarrow 2 * h_{\text{low}} \downarrow 2 \\ \text{HH} = \mathbf{X} * h_{\text{high}} \downarrow 2 * h_{\text{high}} \downarrow 2 \end{cases}$$

where $h_{\text{low}}, h_{\text{high}}$ are orthogonal wavelet filters (e.g., Haar or Daubechies), $*$ denotes convolution, and $\downarrow 2$ indicates downsampling by a factor of 2.

A.2 Relevance Map Construction

To identify spatial regions that require enhanced refinement during generation, we compute a wavelet-based relevance map from the high-frequency subbands. Specifically, we calculate the aggregated energy of the directional detail coefficients:

$$\mathbf{M}_{\text{relevance}} = \text{LH}^2 + \text{HL}^2 + \text{HH}^2$$

This yields a saliency map that highlights localized frequency-rich regions, such as edges, textures, and fine details. The relevance map is then resized to match the original latent resolution via bilinear interpolation and normalized to the range $[0, 1]$:

$$\mathbf{M}_{\text{norm}} = \frac{\mathbf{M}_{\text{relevance}} - \min(\mathbf{M}_{\text{relevance}})}{\max(\mathbf{M}_{\text{relevance}}) - \min(\mathbf{M}_{\text{relevance}}) + \epsilon}$$

where ϵ is a small constant to avoid division by zero.

High-Frequency Subbands The LL subband encodes coarse spatial content and low-frequency structure. While critical for reconstruction, it offers limited information about local complexity or edge activity. In contrast:

- LH, HL, and HH encode gradients and high-frequency variations.
- The aggregated energy of these bands approximates the local gradient magnitude—similar in spirit to edge detectors like Sobel and Laplacian filters.
- This formulation aligns with the intuition that visually salient regions often correspond to areas with rich high-frequency content.

This approach is theoretically supported by prior work in multiscale signal analysis, which demonstrates that the local maxima of wavelet detail coefficients correspond to structural singularities and perceptual boundaries [38]. While we do not explicitly track maxima across scales, aggregating the squared energies of the high-frequency subbands provides a lightweight approximation of local gradient magnitude, serving as an effective, interpretable proxy for visual saliency in latent space.

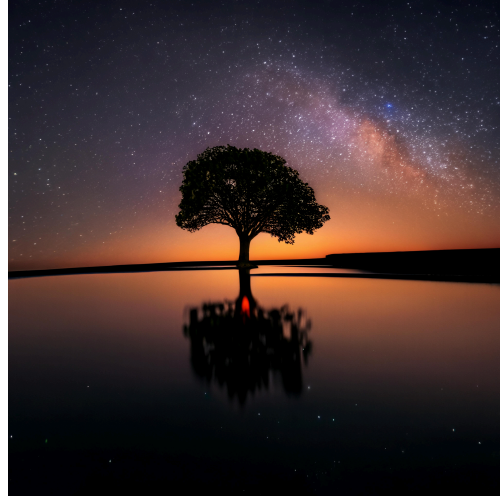
B High Frequencies Suppression

A natural question arises from the apparent tension between our use of a multi-scale VAE loss to suppress high-frequency components in the latent space, and our later use of high-frequency energy to guide the adaptive masking process during diffusion training. While at first glance these two strategies may appear contradictory, they in fact serve complementary and sequential roles in enforcing a more structured and semantically meaningful generative process.

The multi-scale loss used to fine-tune the VAE does not aim to eliminate all high-frequency content. Rather, it penalizes frequency components that are inconsistent across scales, often indicative of reconstruction noise, aliasing artifacts, or signal components that do not correspond to real-world structures in the input image. In this context, high-frequency suppression is not a blanket filtering of detail, but a targeted regularization of spectral instability, with the goal of aligning the latent spectral distribution more closely with that of clean, natural images. By enforcing reconstruction consistency across resolutions and stabilizing spectral decay (e.g., toward a natural $1/f^2$ power law), the VAE is



A man with an afro hairstyle wears futuristic reflective sunglasses and a coat with fur lining, standing in front of a vibrant pink and blue neon sign.



A lone tree stands in calm water reflecting the starry night sky, with the Milky Way stretching above and warm orange hues from a distant horizon.



A young astronaut in a light-colored suit stands in a vibrant field of wildflowers, holding a helmet and gazing upward, with a warm, glowing sunset in the background.



A person wearing a Spider-Man suit in the game Half-Life Alyx."

Figure 6: Images generated at 4K resolution with LWD+SANA.

encouraged to encode only those high-frequency components that are structurally and semantically grounded in the image content.

Crucially, it is precisely this filtered latent space that makes frequency-based attention meaningful. Once the latent tensor has been regularized to remove spurious high-frequency noise, the remaining high-frequency energy, extracted via wavelet decomposition, is more strongly correlated with visually salient features such as edges, object boundaries, fine textures, and local geometric complexity. In other words, by denoising the latent representation, the VAE enhances the signal-to-noise ratio of the wavelet attention mechanism. This enables the diffusion process to make effective use of frequency-aware masking, prioritizing spatial refinement in regions that contain real, informative structure, rather than noise. Without this preceding spectral refinement, attention maps derived from high-frequency energy would risk being dominated by latent artifacts or encoder instability, thus undermining the selective refinement objective of our method.

This sequential design, first purifying the latent space, then exploiting its structured frequency characteristics, ensures that our method combines the strengths of signal-domain regularization and content-adaptive computation in a theoretically grounded and practically synergistic manner.



A surreal landscape depicting an ethereal fusion of natural beauty and fantastical architecture, reminiscent of Salvador Dalí's dreamlike paintings. From above the clouds, one gazes upon a colossal tower emerging from the earth, its intricate gears visible as it merges seamlessly with a tranquil mountain lake. The scene is bathed in an otherworldly glow, casting lavender and gold hues across the sky, while delicate cherry blossoms flutter gently in the foreground, adding a sense of serenity to this breathtaking vision where time and nature intertwine.



Steampunk airship floating above a misty Victorian cityscape, intricate brass and copper mechanical details, golden hour lighting, billowing clouds, detailed architectural elements, rich warm color palette, cinematic composition.

Figure 7: Images generated at 4K resolution with LWD+URAE.



Girl with pink hair, vaporwave style, retro aesthetic, cyberpunk, vibrant, neon colors, vintage 80s and 90s style, highly detailed.



A sleek black luxury sedan parked on a rain-soaked city street at night, reflecting neon lights from nearby buildings. The wet pavement glistens, and the car's smooth curves are highlighted by the ambient glow of the urban environment.



A narrow and picturesque alley in the historic center of Naples, with laundry hanging out to dry between flower-filled balconies and the inviting aroma of freshly baked pizza in the air.

Figure 8: Images generated at 4K resolution with LWD+URAE.

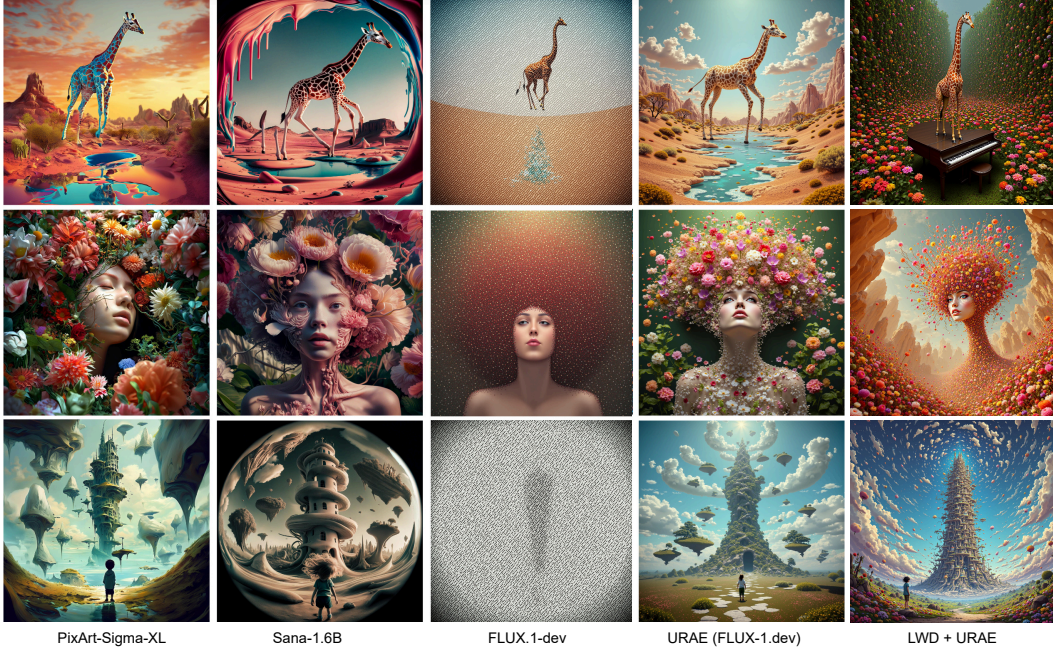


Figure 9: Visual comparison of 4K image generations from LWD and competing baselines.

C Additional Results for 4K

To assess the efficacy of our proposed Latent Wavelet Diffusion (LWD), we conduct a detailed evaluation focusing on the challenging 4K resolution (4096×4096).

C.1 Quantitative Results

Table 3 presents the quantitative comparison on 4K image generation. We evaluate the generated images using several key metrics: MAN-IQA [67] and QualiCLIP [2], which assess perceptual image quality and alignment with textual prompts, respectively. Additionally, we compute the GLCM (Gray-Level Co-occurrence Matrix) score as a measure of texture complexity and detail richness in the generated high-resolution outputs. Finally, we report the Compression Ratio, indicating the compressibility of the generated images, which can be indicative of redundancy or lack of fine details.

Our LWD-enhanced URAE demonstrates competitive performance across all evaluated metrics. Notably, it achieves the highest MAN-IQA score and GLCM score, suggesting superior perceptual quality and richer textural details compared to the baselines. Furthermore, our LWD + URAE achieves a favorable Compression Ratio (28.77), better than URAE and PixArt-Sigma-XL, suggesting a good balance between detail and redundancy. These quantitative results underscore the effectiveness of our LWD approach in enhancing the visual quality and detail of images generated at 4K resolution.

C.2 Qualitative Analysis

To complement the quantitative evaluation, Figures 10, 11, 13, and 12 provide a qualitative comparison of LWD against selected baselines, presenting side-by-side comparisons of the generated images.

The visual comparisons highlight the benefits of our LWD enhancement. Our method demonstrates the generation of images with finer and more intricate details, particularly noticeable in complex textures and object boundaries. These qualitative observations align with our quantitative findings, reinforcing the effectiveness of the proposed LWD for high-resolution image generation.



URAE

LWD + URAE

Figure 10: 4K generation of URAE vs LWD + URAE.

Upper caption: "Eiffel Tower was Made up of more than 2 million translucent straws to look like a cloud, with the bell tower at the top of the building, Michel installed huge foam-making machines in the forest to blow huge amounts of unpredictable wet clouds in the building's classic architecture."
Lower caption: "Barbarian woman riding a red dragon, holding a broadsword, in gold armour."

Table 3: Evaluation on ultra resolution (4096 × 4096) image generation task with [64] prompts.

| Method | MAN-IQA (↑) | QualiCLIP (↑) | GLCM Score ↑ | Compression Ratio ↓ |
|---------------------|---------------|---------------|--------------|---------------------|
| PixArt-Sigma-XL [9] | 0.2935 | 0.2308 | 0.48 | 45.15 |
| Sana-1.6B [65] | 0.3288 | 0.4979 | <u>0.71</u> | 25.89 |
| FLUX-1.dev [31] | 0.3673 | 0.2564 | - | - |
| URAE [69] | <u>0.3850</u> | 0.3758 | 0.41 | 38.86 |
| LWD + URAE | 0.4011 | <u>0.3855</u> | 0.74 | <u>28.77</u> |

D Frequency-Aware Evaluation

To rigorously assess the frequency characteristics of generated images, we propose a suite of frequency-sensitive metrics that extend beyond standard perceptual scores. These metrics are designed to quantify the degree to which generated images preserve the natural frequency distribution observed in real images, with particular attention to the presence and quality of high-frequency details.

High/Low Frequency Ratio (HLFR): We decompose each image using a 2D discrete wavelet transform (DWT) and compute the total energy in the detail coefficients (high-frequency subbands: LH, HL, HH) and in the approximation coefficients (low-frequency LL subband). The HLFR is defined as the ratio of high-frequency to low-frequency energy:

$$\text{HLFR} = \frac{E_{LH} + E_{HL} + E_{HH}}{E_{LL}}.$$

This ratio reflects the relative emphasis on fine-scale structures. A value similar to the reference (real images) indicates a natural distribution of frequency content. Large deviations can signal oversmoothing or hallucinated detail.

Ratio Difference from Real (RDR): To quantify deviation from the natural HLFR, we compute the absolute difference between the HLFR of the generated image and the real reference:

$$\text{RDR} = |\text{HLFR}_{\text{gen}} - \text{HLFR}_{\text{real}}|.$$

Lower values are better, indicating better alignment with the natural frequency distribution.

Wavelet Quality Score (WQS): This metric evaluates the structural similarity between generated and real images in the wavelet domain, where frequency components are explicitly separated by scale and orientation. Given a multi-level discrete wavelet transform (DWT) of both the generated image I_g and the reference image I_r , we compute the SSIM and MSE for each corresponding subband s across all decomposition levels l . The final WQS aggregates the per-subband scores using frequency-aware weights:

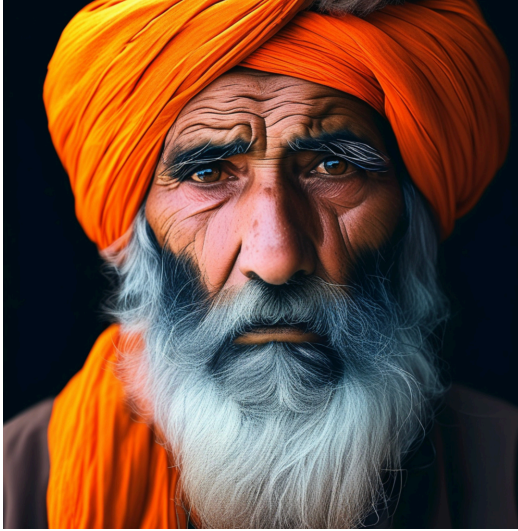
$$\text{WQS} = \sum_{l=1}^L \sum_{s \in \{LL, LH, HL, HH\}} w_{l,s} \cdot \text{SSIM}(I_r^{l,s}, I_g^{l,s}) - \lambda \cdot \text{MSE}(I_r^{l,s}, I_g^{l,s}),$$

where $w_{l,s}$ are weights that can prioritize perceptually important subbands (e.g., low-frequency LL or high-frequency HH), and λ is a scaling factor that penalizes distortion. The score is normalized to $[0, 1]$, where 1 indicates perfect structural alignment. Higher WQS values reflect better reconstruction fidelity across frequency scales, meaning the model preserves both coarse structure and fine texture.

High-Frequency Energy (HFE): This metric quantifies the total energy of the image’s high-frequency components after wavelet decomposition. For a given decomposition level, we define:

$$\text{HFE} = \sum_{l=1}^L (\|I^{l,LH}\|^2 + \|I^{l,HL}\|^2 + \|I^{l,HH}\|^2).$$

This value provides an absolute measure of fine-scale activity in the image. While real images have characteristic HFE ranges, excessive HFE may indicate artifacts or noise, and too little HFE suggests oversmoothing. Alignment with the real HFE is typically ideal.



PixArt-Sigma-XL

LWD + PixArt-Sigma-XL

Figure 11: 2K generation of PixArt-Sigma-XL vs LWD + PixArt-Sigma-XL.
Upper caption: "An elderly man with a prominent, bushy beard and deep-set eyes wears a vibrant orange turban, his weathered face marked by lines of age and experience.". Lower caption: "A lone figure on a horse stands in a misty forest, gazing up at a tall, multi-tiered temple surrounded by towering trees and soft, diffused light. Steam rises from the rocks near a stream, creating an atmospheric scene of tranquility and mystery."

Table 4: Comparison of frequency-sensitive metrics across different methods on Aesthetic-4K [71] validation set.

| Metric | HLFR | RDFR ↓ | WQS ↑ | HFE | HFEI ↓ | FSIM ↑ | MS-SSIM ↑ |
|-----------------------|---------------|---------------|---------------|---------------|---------------|---------------|---------------|
| Real | 0.0560 | 0.0000 | 1.0000 | 0.0140 | 0.0000 | 1.0000 | 1.0000 |
| Sana-1.6B [65] | 0.0784 | 0.0558 | 0.4673 | 0.0196 | 0.6108 | 0.6128 | 0.1324 |
| LWD + Sana-1.6B | 0.0610 | 0.0537 | 0.4701 | 0.0144 | 0.5227 | 0.6217 | 0.1324 |
| SD3-Diff4k-F16 [71] | 0.0691 | 0.0470 | 0.4624 | 0.0158 | 0.8064 | 0.6155 | 0.1296 |
| LWD + SD3-F16 | 0.0555 | 0.0437 | 0.4735 | 0.0144 | 0.4826 | 0.6245 | 0.1521 |
| PixArt-Sigma-XL | 0.0550 | 0.0409 | 0.4763 | 0.0119 | 0.6296 | 0.1354 | 0.4255 |
| LWD + PixArt-Sigma-XL | 0.0564 | 0.0500 | 0.4730 | 0.0150 | 0.6239 | 0.1478 | 0.5094 |

High-Frequency Emphasis Index (HFEI): This metric evaluates how much the model over- or under-emphasizes high-frequency content relative to the real distribution. We define it as:

$$\text{HFEI} = \left(\frac{\text{HFE}_{\text{gen}}}{\text{TotalEnergy}_{\text{gen}}} \right) - \left(\frac{\text{HFE}_{\text{real}}}{\text{TotalEnergy}_{\text{real}}} \right),$$

where total energy is computed over all wavelet subbands. $\text{HFEI} > 0$ indicates the generated image places more emphasis on high frequencies than real images (potentially hallucinated detail), while $\text{HFEI} < 0$ indicates a loss of fine detail. An HFEI near zero is ideal.

Perceptual Metrics: For completeness, we also report FSIM [72] and MS-SSIM [62], which capture visual similarity and structural coherence, respectively. Both metrics are bounded between 0 and 1, with higher values indicating better perceptual quality.

Results: Table 4 summarizes the performance of diffusion backbones, along with their respective versions enhanced with LWD. LWD consistently improves frequency alignment: for instance, the LWD+Diff4K variant achieves a high/low frequency ratio of 0.0556, nearly identical to the real reference (0.0560), while also minimizing the ratio difference (0.0438). Wavelet Quality Scores improve in both cases, and the HF energy is more tightly controlled, preventing oversharpening. Importantly, LWD preserves or improves FSIM and MS-SSIM, confirming that frequency fidelity does not come at the expense of perceptual quality. These results demonstrate that LWD enhances the frequency realism of generated images in a measurable and interpretable way, offering a principled approach to frequency-aware image synthesis.

E Effect of Scale-Consistency Loss on Reconstruction Quality

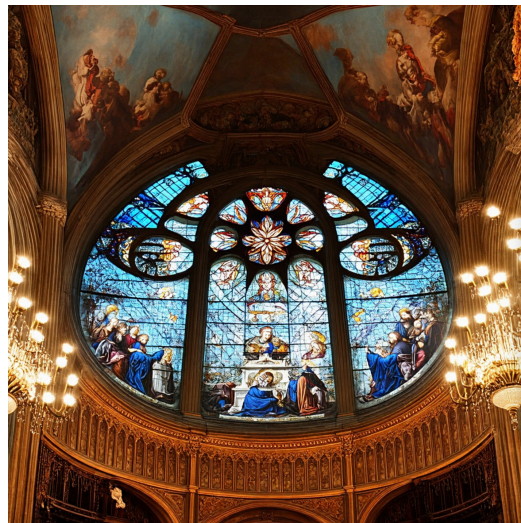
Table 5 reports quantitative reconstruction metrics for various VAEs, with and without the proposed Scale-Consistency (SC) loss, evaluated on the Aesthetic-4K validation set. Across different architectures SD3-VAE, Flux-VAE, and Sana-AE, the addition of SC consistently improves performance, particularly in rFID and perceptual quality (LPIPS). For instance, Flux-VAE-SC outperforms its baseline with a significant reduction in rFID (0.50 vs. 0.73) and an increase in PSNR and SSIM, indicating sharper and more faithful reconstructions. Notably, SD3-VAE-F16-SC achieves a substantial LPIPS improvement (0.18 vs. 0.30), suggesting better perceptual fidelity despite using a more aggressive compression factor (F16). These results confirm that scale-consistent regularization enhances latent representations, making them more robust and structurally aligned, critical properties for downstream diffusion tasks.



Figure 12: 4K generation of Sana vs LWD + Sana.
 Upper caption: "A litter of golden retriever puppies playing in the snow. Their heads pop out of the snow, covered in.". Lower caption: "A curvy timber house near a sea, designed by Zaha Hadid, represent the image of a cold, modern architecture, at night, white lighting, highly detailed."

Table 5: Quantitative reconstruction results of VAEs with and without the Scale-Consistency Loss 3.1 on Aesthetic-4K [71] validation set.

| Model | rFID ↓ | NMSE ↓ | PSNR ↑ | SSIM ↑ | LPIPS ↓ |
|------------------|-------------|-------------|--------------|-------------|--------------|
| SD3-VAE [13] | 1.05 | 0.01 | 26.54 | 0.86 | 0.08 |
| SD3-VAE-F16 [71] | 0.70 | 0.07 | 19.82 | 0.63 | 0.30 |
| SD3-VAE-F16-SC | 0.70 | 0.04 | 22.58 | 0.75 | 0.18 |
| Flux-VAE [31] | 0.73 | 0.01 | 27.18 | 0.89 | 0.07 |
| Flux-VAE-SC | 0.50 | 0.01 | 28.14 | 0.90 | 0.06 |
| Sana-AE [65] | 0.74 | 0.04 | 22.16 | 0.70 | 0.159 |
| Sana-AE-SC | 0.55 | 0.02 | 23.64 | 0.73 | 0.163 |



SD3-Diff4k-F16

LWD + SD3-F16

Figure 13: 2K generation of SD3-Diff4k-F16 vs LWD + SD3-F16.

Upper caption: "A serene landscape features a winding river, flanked by trees with autumn foliage, leading to a rustic wooden cabin with a corrugated roof, set against a softly blurred background."
Lower caption: "A grand interior featuring intricate stained glass windows, an elaborate rose window, ornate frescoes depicting biblical scenes, and elegant chandeliers illuminating the richly decorated walls and arches."